archives
of thermodynamics
Vol. **39**(2018), No. 1, 147–166
DOI: 10.1515/aoter-2018-0008

Thermal and hydraulic phenomena in boundary layer of minijets impingement on curved surfaces

TOMASZ KURA[a]
ELŻBIETA FORNALIK-WAJS[a*]
JAN WAJS[b]

[a] AGH University of Science and Technology, Faculty of Energy and Fuels, Department of Fundamental Research in Energy Engineering, 30 Mickiewicza Avenue, 30-059 Krakow, Poland

[b] Gdansk University of Technology, Faculty of Mechanical Engineering, Department of Energy and Industrial Apparatus, Narutowicza 11/12, 80-233 Gdańsk, Poland

Abstract Presented work considers flow and thermal phenomena occurring during the single minijet impingement on curved surfaces, heated with a constant heat flux, as well as the array of minijets. Numerical analyses, based on the mass, momentum and energy conservation laws, were conducted, regarding single phase and two-phase simulations. Focus was placed on the proper model construction, in which turbulence and boundary layer modeling was crucial. Calculations were done for various inlet parameters. Initial single minijet results served as the basis for the main calculations, which were conducted for two jet arrays, with flat and curved heated surfaces. Such complex geometries came from the cooling systems of electrical devices, and the geometry of cylindrical heat exchanger. The results, regarding Nusselt number, heated surface temperature, turbulence kinetic energy, production of entropy and vorticity, were presented and discussed. For assumed geometrical parameters similar results were obtained.

Keywords: Jet impingement; Minijets array; Boundary layer; Entropy generation; Nusselt number

*Corresponding Author. Email: elzbieta.fornalik@agh.edu.pl

Nomenclature

c_p	–	specific heat, J/(kg K)
d	–	orifice diameter, m
E	–	total energy, J
H	–	jet height, m
k	–	turbulence kinetic energy, m^2/s^2
m	–	fluid mass, kg
$\dot{m}$	–	mass transfer between phases (mass flow rate), kg/s
Nu	–	Nusselt number
p	–	pressure, Pa
Pr	–	Prandtl number
q	–	heat flux, W/m^2
R	–	curvature radius, m
Re	–	Reynolds number
S	–	distance between jets, m
$\dot{s}_{gen}$	–	rate of specific entropy generation, W/(kg K)
S_{ij}	–	strain rate tensor, 1/s
T	–	temperature, K
t	–	time, s
u	–	velocity, m/s
u^*	–	friction velocity, m/s
$\overline{u_i' u_j'}$	–	Reynolds stress term, m^2/s^2
V	–	volume, m^3
x	–	distance from stagnation point, m
y	–	distance to the nearest wall, m
y^+	–	dimensionless wall distance

Greek symbols

α	–	convective heat transfer coefficient, $W/(K\,m^2)$
β	–	volume fraction
ε	–	turbulence dissipation rate, W/kg
λ	–	thermal conductivity, W/(K m)
μ	–	dynamic viscosity, Pa s
ν	–	kinematic viscosity, m^2/s
ρ	–	density, kg/m^3
φ	–	viscous dissipation function

Subscripts

1	–	primary phase
2	–	secondary phase
ef	–	effective (regarding turbulence modeling)
p	–	value at the first near-wall node
w	–	value at wall
$\bar{(\cdot)}$	–	time averaged value

1 Introduction

Considering the thermodynamical, ecological, and economical aspects of operating and planned installations, the subject of heat transfer enhancement will usually be raised. It is very important issue, since the demand for high heat fluxes transfer comes for example from progressive miniaturization of devices. It is also caused by the demand for low-temperature heat sources utilization or development of the system for dispersed power generation, for example vapour units of combined heat and power (CHP) plants [1,2]. New ideas for efficient processes are inevitable.

The idea of heat transfer intensification by jet impingement is not new. This method is successfully applied for example in many metallurgical processes. It was also introduced to the novel construction of heat exchanger [3], giving very good results in transferred heat rates and lower than in other similar devices hydraulic resistance [4,5]. The impingement heat transfer is caused by the modification of boundary layer. Additionally, when the crossflow appears, the heat and mass transfer becomes very complex. The numerical investigations of single jet impingement was done for example by Tong [6] and Berberovic [7], who tried to obtain results comparable with experimental work of Stevens [8] and analytical relations found in Liu's publication [9]. In their papers, valuable information concerning the mesh generation and solver configuration could be found. However, authors encountered difficulties in correct prediction of Nusselt number in the stagnation zone of impingement. The paper by Zuckerman and Lior [10] confirmed, that so far most of the available computational fluid dynamics (CFD) codes are unable to predict this important parameter in stagnation zone with absolute correctness. Similar analysis becomes even more challenging when array of jets is being analysed – as the crossflow effects have to be considered. In last few years, numerous articles presented thermal analysis of jets array, such as [11–13]. While all mentioned publications were based on RANS (Reynolds averaged Navier-Stokes) approach of turbulence modeling, with an increase of computation power also large eddy simulation (LES) analyses of more complex systems started to be performed [14]. All listed papers described the impact of jet impingement on flat heat exchanging surface. However, it is important to analyse also impact on other surfaces, such as cylindrical ones. There were no examples of similar numerical work in the literature, taking into account the effects not only of jet impingement but also the crossflow impacting it. Such configuration can be found in mentioned above cylindrical heat exchanger with

minijets technology [3]. Therefore the main aim of the undertaken studies is the construction of numerical model of such array of jets. In the following paper the flow structure and thermal performance of impingement on flat and analogical curved surfaces are presented and compared.

2 Reference case – two-phase minijet

The reference case of the minijet impingement concerned two- and three-dimensional, multiphase analyses. For the purpose of model and mesh validation, transient analyses were performed, conducted with Ansys 15 software, particularly the Fluent module. Geometrical parameters and boundary conditions were taken from the papers [6–8]. Figure 1 presents general view of the reference case, as well as boundary conditions placement. Inlet diameter, d, was equal to 4.06 mm, distance from orifice exit to heated surface was equal to $3.7d$. Depending on the case, heated surface had the length of $10d$ (2D axisymmetric) or $5d$ (3D). Initially, whole area was filled with air, while water was entering the system through the inlet.

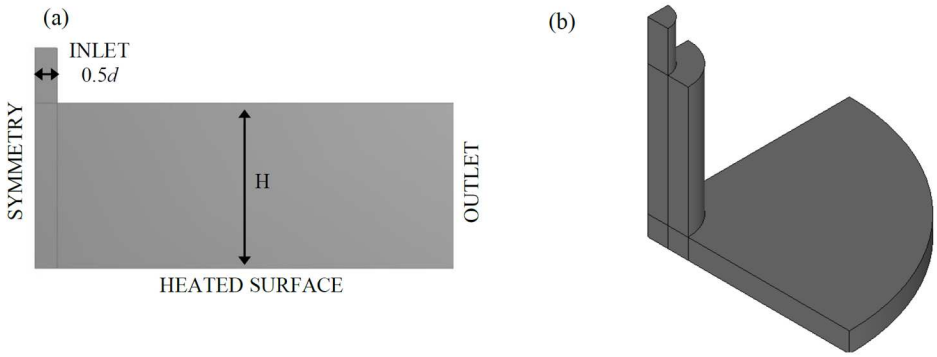

Figure 1: Reference case geometry: (a) – 2D axisymmetric, (b) – 3D.

High resolution, second order discretization schemes were applied to provide reliable results. The conservation laws of continuity, momentum, and energy, coupled with realizable k-ε with enhanced wall function or SST k-ω turbulence (classic and transitional versions) models were considered, with Reynolds averaging approach [15] and enhanced wall treatment:

$$\frac{1}{\rho_2}\left[\frac{\partial}{\partial t}\left(\beta_2\rho_2\right)+\left(\rho_2\frac{\partial\beta_2\overline{u_i}}{\partial x_i}\right)\right]=\dot{m}_{1-2}-\dot{m}_{2-1}\ , \tag{1}$$

$$\rho\frac{\partial\overline{u_i}}{\partial t}+\rho\frac{\partial}{\partial t}\left(\overline{u_j}\overline{u_i}\right)=-\frac{\partial\overline{p}}{\partial t}+\frac{\partial}{\partial t}\left(2\mu S_{ij}-\rho\overline{u_i^{'}u_j^{'}}\right)\ , \tag{2}$$

$$\rho\frac{\partial\overline{E}}{\partial t}+\frac{\partial}{\partial t}\left(\overline{u_i}\left(\rho\overline{E}+\overline{p}\right)\right)=\frac{\partial}{\partial x_j}\left(\lambda_{ef}\frac{\partial\overline{T}}{\partial x_j}\right)\ ,\quad i,j=1,2,3\ , \tag{3}$$

$$\rho=\beta_2\rho_2+(1-\beta_2)\,\rho_1\ , \tag{4}$$

where u is the velocity, ρ is the density, β is the volume fraction, $\dot{m}$ is the mass transfer between phases, p is the pressure, μ is the dynamic viscosity, S_{ij} is the strain rate tensor, $\overline{u_i^{'}u_j^{'}}$ is the Reynolds stress term, E is the total energy, T is the temperature, λ_{ef} is the effective thermal conductivity. Subscripts 1 and 2 denote the primary and secondary phase, respectively, and $i,j=1,2,3$. All variables marked with overline, such as $(\overline{\cdot})$, represent time-averaged value.

Volume of fluid (VOF) scheme was applied as the multiphase model. The most important feature of this method is, that the fields for all variables and properties were shared by the phases and represented volume-averaged values. An additional variable was introduced: the volume fraction of the phase, and the tracking of the interface between phases was accomplished by the solution of a continuity equation for the volume fraction of secondary phase (its choice is arbitrary). The common density in each cell was calculated with Eq. (4).

The air and water were chosen as the working fluids. Their default, software implemented parameters remained unchanged and temperature-independent throughout simulations, to avoid increase of computational time. It was verified, that impact of their change on obtained results was negligible. Analyses started with 2D axisymmetric model of one water minijet hitting the flat surface through air-filled zone. It was followed by the 3D model. Inlet velocity was defined on the basis of the Reynolds number:

$$\mathrm{Re}=\frac{\rho u d}{\mu}\ , \tag{5}$$

where d is the characteristic length, the orifice diameter in the case of jet impingement.

Table 1 presents boundary conditions for this case, analogical to the papers [6–8]. Inlet turbulence intensity value was set at the level of 5%, as the flow was initially turbulent.

Table 1: Boundary conditions – reference case.

Inlet Reynolds number	Inlet water temperature, K	Initial air temperature, K	Heat flux at the surface, W/m^2
10600	283	283	149000

The most important preliminary task was to fulfil the mesh requirements concerning jet impingement (e.g., distance between the wall and first calculation node). These requirements were coming from proper representation of published data. Process of mesh construction was time consuming and combined both theoretical and trial-errors approaches and conducted of typical mesh independence tests. The final space division was chosen basing on the comparison of obtained results with [6–8]. Two parameters were chosen to verify the correctness of the model, the liquid film height and the local Nusselt number distribution along the heated surface. Their values were controlled to assure achieving of steady state solution. First one was used to check proper flow behaviour, second one to check thermal performance of the model. Nusselt number was defined as

$$\mathrm{Nu} = \frac{\alpha d}{\lambda}, \tag{6}$$

where α is the convective heat transfer coefficient. It was determined in the basis of Newton's law [15]:

$$\alpha = \frac{q_w}{T_w - T_p}, \tag{7}$$

where q_w is the heat flux at the wall, T_w is the temperature at the wall, and T_p is fluid's temperature at the first near-wall node. Temperature of the wall was calculated in iterative manner from assumed constant heat flux boundary condition and turbulence modeling.

The most important factor characterizing boundary layer, y^+, is defined as follows:

$$y^+ = \frac{u^* y}{\nu}, \tag{8}$$

where u^* is the friction velocity, y is the distance to the nearest wall, and ν is the kinematic viscosity of the fluid.

Figure 2 presents the calculated liquid film height comparison for analysed cases, at given distance x from the stagnation point. As it can be seen, difference between them and the results from [6] are negligible. Such effect, however, was achieved only, when transitional SST k-ω model was applied, with mesh in which y^+ value at every first node near the wall was equal or smaller than 1. Therefore results for realizable k-ε model simulations are not presented here, and 2D and 3D cases were calculated at $y^+ = 1$.

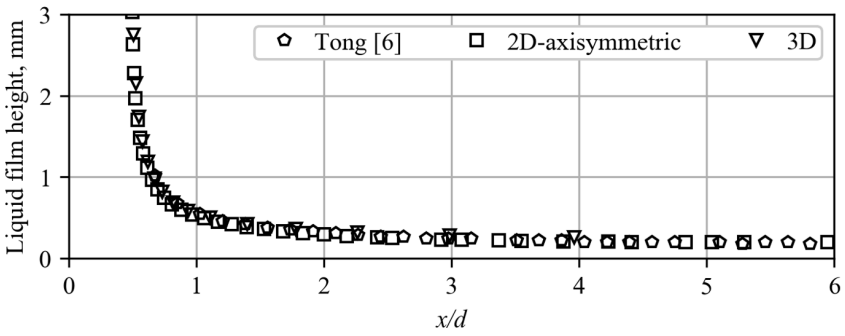

Figure 2: Liquid film height comparison.

Figure 3 presents similar comparison, regarding local Nusselt number distribution along the heated surface, in reference to corresponding values from [7] and [8]. The effect of various y^+ values of the mesh near the impinged wall is presented. It can be observed, that only very dense mesh, with y^+ of about 0.5 near the wall, which corresponded to the first cell height of approximately 1.5×10^{-6}m, led to comparable results. The mesh requirements were therefore more demanding for thermal parameters, than for hydrodynamic. Obtained numerical data sets are presented as points, to make the diagram clearer. Again, only transitional SST k-ω model, with proper y^+, was able to predict Nusselt number distribution properly. Results of Stevens came from experiment [8], and they did not exhibit, in contrast to numerical results, the peak of Nusselt number – this discrepancy, previously mentioned, is the biggest problem of most CFD codes. However, besides that peak, a good agreement with [8] could be found. At this stage of work that discrepancy was acceptable, however future works will be oriented on its reduction. Important fact is, that the heat transfer occurred between water and surface, in the single-phase area – validation presented in Fig. 3 could serve then as a basis for discretization of single-phase models described in Sec. 3 and 4.

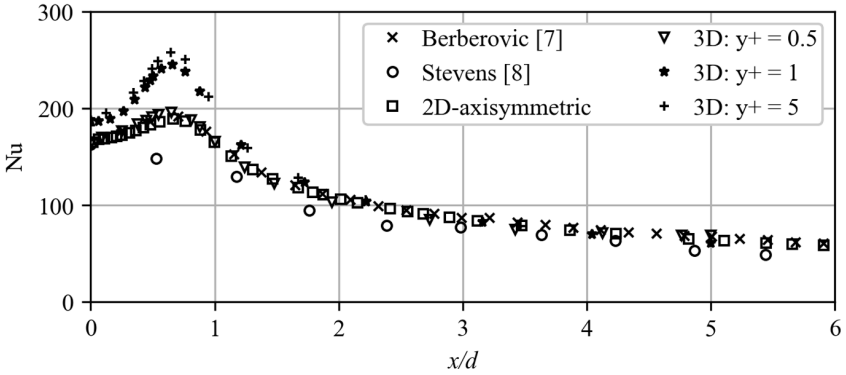

Figure 3: Nusselt number comparison.

3 Single-phase minijet

The main conclusion from Sec. 2 was, that proper heat transfer prediction can be achieved only due to dense and nearly uniform mesh near the surface. In authors' opinion the proposed model predicted all important parameters properly and, with taking into account its main assumptions regarding mesh generation, numerous axisymmetric simulations of one, single-phase minijets impinging on various surfaces (flat and concave type) could be performed. Their boundary conditions, listed in Tab. 2, were chosen to correspond with these used for complex jet array system, described in Tab. 6 in Sec. 4.

Table 2: Boundary conditions – single-phase minijet (water).

Uniform inlet velocity, m/s				Inlet fluid temperature, K	Heat flux at the surface, W/m^2
1.5	4	5	6	293	150000
Corresponding Re in the orifice					
1490	3980	4975	5970		

For the purpose of Sec. 3 and 4 analyses, transient, single-phase (water or air), two-dimensional axisymmetric and three-dimensional analyses were performed. High resolution, second order discretization schemes were applied to provide sufficient results. The conservation laws of mass, mo-

mentum, and energy, coupled with transitional SST k-ω turbulence model and ehnanced wall treatment were considered, with Reynolds averaging approach [15]:

$$\frac{\partial \overline{u_i}}{\partial x_i} = 0 \,, \tag{9}$$

$$\rho \frac{\partial \overline{u_i}}{\partial t} + \rho \frac{\partial}{\partial t} \left(\overline{u_j u_i} \right) = -\frac{\partial \overline{p}}{\partial t} + \frac{\partial}{\partial t} \left(2\mu S_{ij} - \rho \overline{u_i' u_j'} \right) \,, \tag{10}$$

$$\rho \frac{\partial \overline{E}}{\partial t} + \frac{\partial}{\partial t} \left(\overline{u_i} \left(\rho \overline{E} + \overline{p} \right) \right) = \frac{\partial}{\partial x_j} \left(\lambda_{ef} \frac{\partial \overline{T}}{\partial x_j} \right) \,, \quad i, j = 1, 2, 3 \,. \tag{11}$$

The main goal of such simulations was to investigate, wheather the influence of surface shape on heat transfer efectiveness can be correlated with some gometrical parameters – which might be useful for more complex geometries. The jet characteristics taken from [2–5] and discussed later in Sec. 4, where the orifice diameter, d, equal to 1 mm, the distance between orifice and impinged surface H equal to 2 mm and surface curvature radius, R, equal to 8 mm, was compared with other geometrical configurations, listed in Tab. 3. As in the heat exchanger, water was taken as the working fluid. The air was considered for the purpose of additional model validation. Generated mesh fulfilled the requirements described in the previous section, giving very good agreement with the literature.

Table 3: Geometry details of all analyzed single-phase minijet cases (water).

Surface	Orifice Re	Orifice diameter d, mm			H/d	R/d
FLAT	3980	1			1.5, 2, 2.5	–
	4975				1.5, 2, 2.5	
	5970				1.5, 2, 2.5	
CONCAVE	1490	1			1.5, 2, 2.5	1.5, 2, 4, 6, 8
	3980				1.5, 2, 2.5	
	4975				1.5	
		1	1.5	2	2	
		1			2.5	
	5970				1.5, 2, 2.5	

In addition to discussed data, the stagnation point Nusselt number, in the case of the flat surface impinging, was compared (see Tab. 4) with the

values obtained by Brdlik and Savin [16] correlation

$$\mathrm{Nu} = 0.82\mathrm{Pr}^{1/3}\mathrm{Re}^{1/2} \,, \tag{12}$$

the Prandtl number is defined as follows:

$$\mathrm{Pr} = \frac{c_p \mu}{\lambda} \,, \tag{13}$$

where c_p is specific heat.

Table 4: Flat surface impingement; comparison of stagnation point Nusselt number obtained by correlation (12) and numerical analyses of single-phase minijet (water).

Re	$\mathrm{Nu}_{correlation}$	$\mathrm{Nu}_{numerical}$		
		H		
		1.5 mm	2 mm	2.5 mm
1490	61	63	62	62
3980	99	97	97	96
4975	110	108	109	110
5970	121	120	120	121

Results from Tab. 4 were also presented in Fig. 4. In general, values obtained numerically are in very good agreement with correlation based ones. Moreover, to test flexibility of the model, three additional cases were investigated, where air was used as the working fluid, and compared with the results obtained with water as the working fluid. Obtained values of stagnation point Nusselt number are listed in Tab. 5. They were normalized, according to the suggestion by Womac *et al.* [17], with the following expression:

$$\mathrm{Nu}_{\mathrm{normalized}} = \frac{\mathrm{Nu}}{\mathrm{Pr}^{0.4}} \,. \tag{14}$$

As can be noticed, there is a small difference in results, however constant for all cases. Such differences were described in the literature, for example in the paper by Womac [17]. It can be stated, that, as mentioned in many publications, stagnation Nusselt number is independent of the working fluid.

Table 5: Comparison of numerically obtained stagnation point Nusselt number with different working fluids for single-phasse minijet calculations.

CASE	$Nu_{normalized}$	
	water	air
FLAT, Re = 4975, H = 2 mm, d = 1mm	50	53
CONCAVE, Re = 4975, H = 2 mm, d = 2 mm, R = 4 mm	37	41

Figure 4 presents the stagnation Nusselt number for analyzed cases of water with constant orifice radius, d, equal to 1 mm, and variable jet height, H, and curvature diameter, R, for concave geometry. Axes were adjusted to present actual differences between Reynolds number values. Presented results were almost independent of H/d. The effect of curvature was vanishing with increase of its radius, starting from $R \geq 6d$ and it could be stated, that for the values of $R \geq 8d$ it should not be visible. An irregular behavior of Nusselt number values in relation to decreasing curvature radii could be noticed. It was caused by the fact, that when the radius of the curved concave surface was too small, generated swirl was impacting the jet itself, breaking its core. Moreover, it could be noticed, that values for the lowest Reynolds number cases slightly differed from the rest, giving also smaller differences between obtained Nusselt number values. In general, however, almost linear relation of Nusselt and Reynolds numbers can be seen. Also, the most important conclusion is, that for all presented cases even with negligible curvature effect, obtained results for the stagnation Nusselt number did not correspond with the flat case results (Tab. 5). For concave geometry they were lower.

Next calculations were conducted to verify, if obtained stagnation Nusselt number values would remain the same with the constant curvature radius to orifice diameter ratio R/d. For that purpose two additional diameters of orifice were used, equal to 1.5 mm and 2 mm, respectively. Analyzed ratios of R/d were equal to 2, 4 and 8. Jet height, H, was kept constant, equal to 2 mm, as well as orifice Reynolds number, equal to 4975. Obtained results are presented in Fig. 5. As it can be seen, there is only a slight difference between the results for particular ratios. Therefore, the stagnation point and mean Nusselt number values might be correlated with this non-dimensional relation for the flat surfaces [17] and the concave ones.

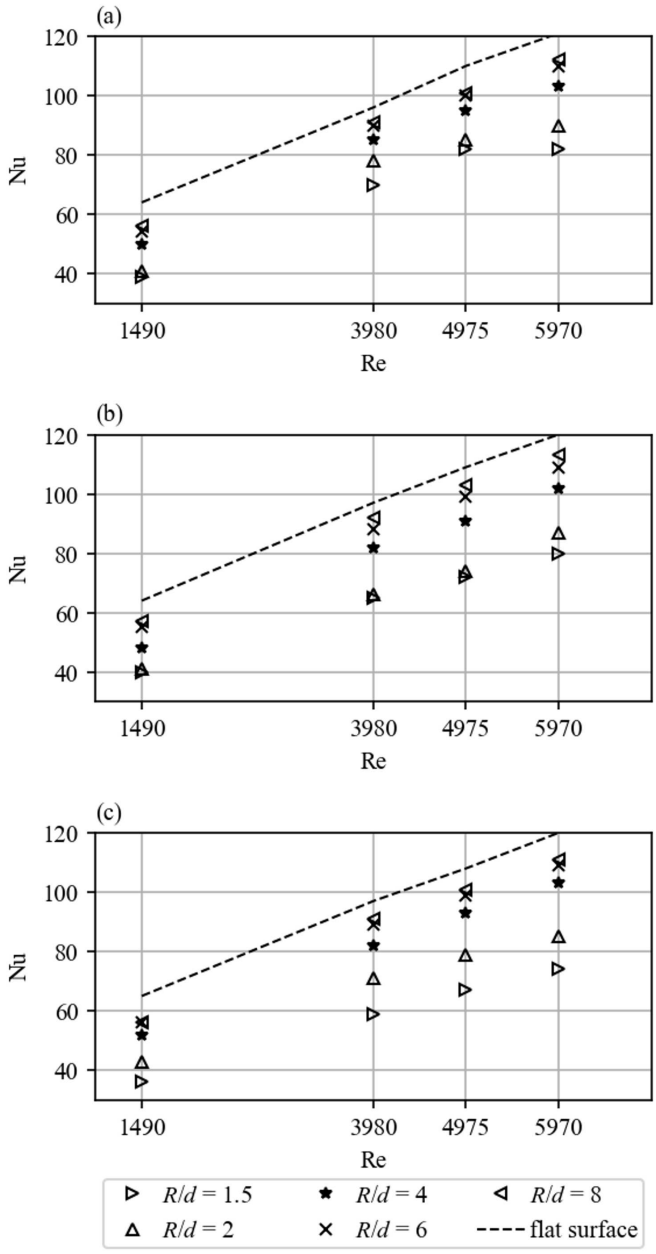

Figure 4: Flat and concave surface single-phase minijet (water) impingement, constant d=1mm, variable H/d and R/d: (a) $H/d = 1.5$, (b) $H/d = 2$, (c) $H/d = 2.5$.

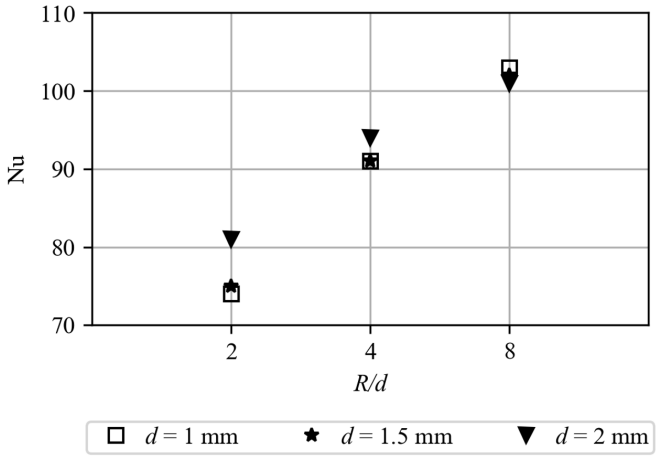

Figure 5: Concave surface, values of stagnation Nusselt number, Nu, for constant R/d ratio, with variable orifice diameter d; H = 2mm, Re = 4975, single-phase minijet (water).

4 Single-phase minijets array

The results obtained when simulating one single-phase minijet impingement (Fig. 4) suggested, that a particular ratio of surface curvature and orifice diameter exists, when the stagnation point Nusselt number variation, with the ratio increase, no longer occurs. Following section discusses the case, in which not only one jet, but a whole array is impacting the surface, with the model geometries based on actual existing heat exchanger [4,5]. In this paper, flat type geometry of minjets array will be described as type 'A' and cylindrical type geometry will be described as type 'B'. Parameters listed in Tab. 6 were chosen to simulate conditions from [4,5]. Difference in the Reynolds number between boundary conditions from Sec. 3 and 4 comes from various origin parameters (velocity or flow rate), used for calculations. It did not affect the quality of results comparison, because, as proven in Sec. 3 of this paper, relation between Nusselt and Reynolds numbers is consistent for the whole tested range. The mathematical model remained the same, as in Sec. 3.

For both cases inlet turbulence intensity was set only to 1%, as the turbulence level was supposed to increase in the orifices. The Reynolds number values, defined as ratio of fluid velocity and jet diameter to its viscosity, were obtained based on mean velocity values at the exit of all orifices.

Table 6: Boundary conditions – single-phase minijets arrays.

	Inlet volume flow rate, l/h				Inlet water temperature, K	Heat flux at the surface, W/m^2
Type A and B heat exchangers	100	200	300	400	293	150000
	Corresponding average orifice velocity, m/s					
	1.12	2.27	3.44	4.62		
	Corresponding mean Re in the orifice					
	1115	2260	3430	4600		

Taking into account all the requirements mentioned in the description of validation process, it was possible to prepare mesh suitable for complex system of microjets impinging the flat and concave surfaces. Figure 6 presents both geometries, with detailed view of the area with orifices. A and B type exhangers have the length of 21 mm. Models were slightly extended, as seen in the figures, to reduce the impact of sudden channel end. Application of the symmetry boundary conditions was very important to assure high quality mesh and reduce calculation time. All orifices generating jets had diameter of 1 mm, and the distance between their exit and heated surface was equal to 2 mm. Distance between the jets had the value above 4 mm. Inlet area for both cases was the same to assure that the velocities corresponding with the inlet volume flow rate remained similar. The geometry of B type was taken from [4,5], with the constant ratio of surface curvature to orifice radius, R/d, equal to 8. The heat exhanger of A type was based on B geometry, but with the flat surface. Heat transfer area was equal to 1.89×10^{-4}m^2. For the reference case, generated mesh consisted only of quadrilateral (2D) or hexahedral (3D) elements, but it was impossible to maintain such regular shapes for the meshes representing heat exchangers. In their cases, tetrahedrons and pyramids were applied in most of the volume, to obtain smooth transition from small orifices to the rest

of geometry. However, hexahedral elements were applied near the heated surface, with proper y^+ parameter kept constant, to provide accurate thermal calculations. Table 7 includes number of elements for two considered cases.

Table 7: Number of mesh elements.

A type heat exchanger	B type heat exchanger
6 303 438	5 882 459

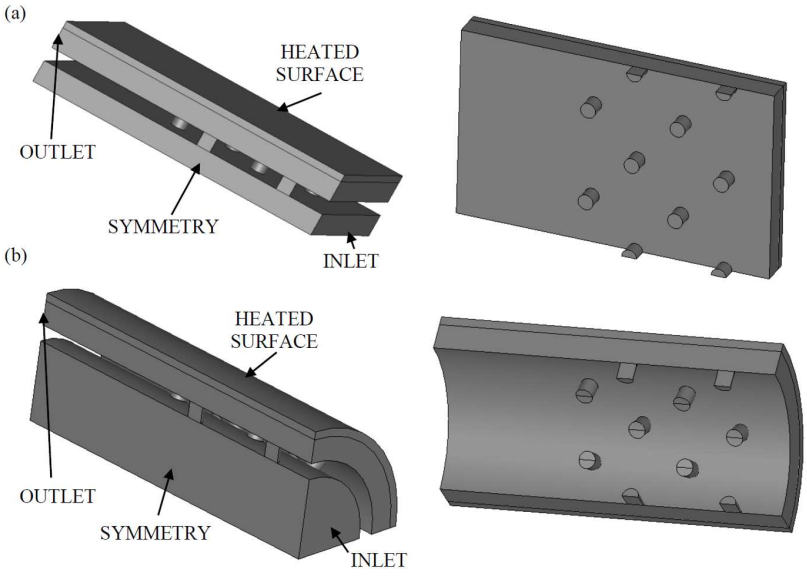

Figure 6: (a) – type A heat exchanger, (b) – type B heat exchanger.

Figure 7 presents the surface average and surface maximum values of Nusselt number on heated surfaces for all analysed cases, as well as surface maximum temperature values. As it can be seen, only small differences of all these values occurred. For lower volume flow rates, maximal values of Nusselt number were higher for type B, but for higher flow rates the tendency was opposite. It suggested, that for such small geometry curvature did not modify the flow behaviour and thermal characteristics significantly. Both cases turned out to be very similar.

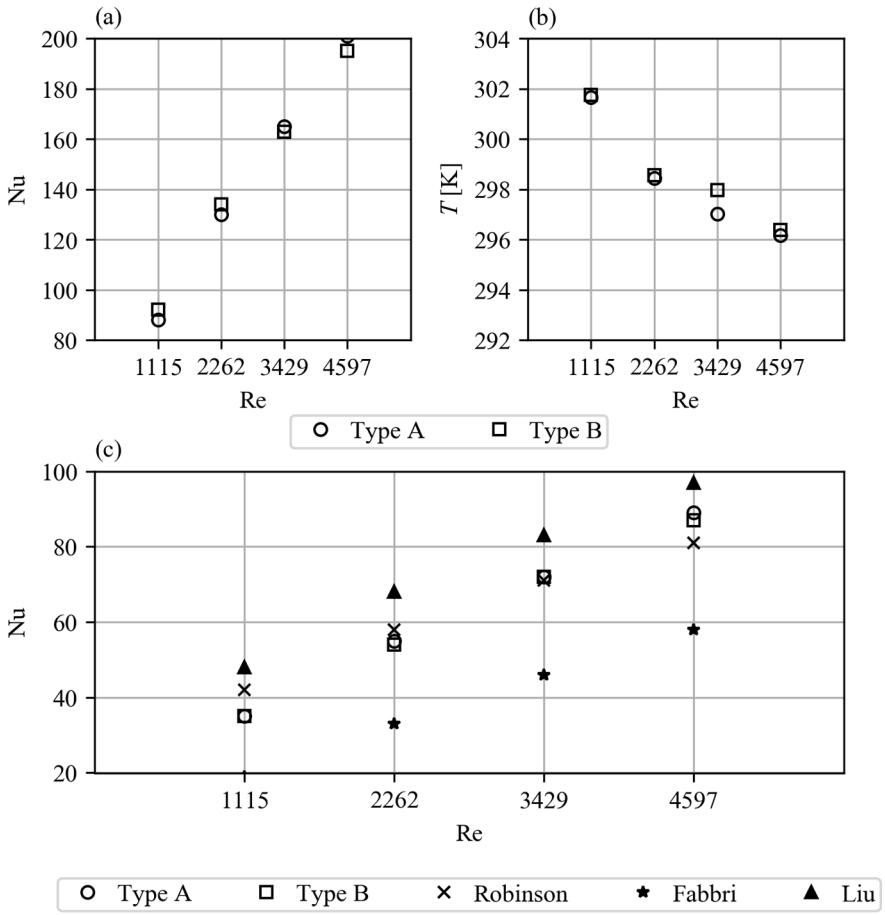

Figure 7: (a) – maximum value of Nusselt number on heated surface, (b) – maximum value of temperature on heated surface, (c) – comparison of mean surface Nusselt number value with correlations.

Also, in Fig. 7, the comparison of obtained results with correlations from literature [9,18,19] concerning similar cases is shown. Table 8 presents mentioned equations, regarding their limitations. None of them considered the curvature radius, R, as the parameter. As already pointed out, it is difficult to find in literature examples of correlations using such factor. Values obtained by Robinson and Schnitzler [18] equation were the closest to the simulation results.

Table 8: Average Nusselt number correlations.

Reference	Nusselt correlation	Limitations
Liu *et al.* [9]	$\mathrm{Nu} = 0.745 Re^{0.5} \mathrm{Pr}^{1/3}$	laminar jets
Robinson and Schnitzler [18]	$\mathrm{Nu} = 1.4853 Re^{0.46} \mathrm{Pr}^{0.4} \left(\frac{S}{d}\right)^{-0.0442} \left(\frac{H}{d}\right)^{-0.00716}$	$650 \leq \mathrm{Re} \leq 6500$ $3 \leq S/d \leq 7$
Fabbri and Dhir [19]	$\mathrm{Nu} = 0.043 \mathrm{Re}^{0.78} \mathrm{Pr}^{0.48} \exp\left(-0.069 \frac{S}{d}\right)$	$43 \leq \mathrm{Re} \leq 3813$ $4 \leq S/d \leq 26.2$

As the thermal parameters did not indicate clearly the differences between A and B type heat exchangers, rate of entropy generation was added as another comparison parameter to identify possible discrepancies. It was useful, as the results might be extended to analyses of more complex models. Rate of specific entropy generation consists of three terms, due to the normal viscous dissipation, turbulence dissipation and thermal dissipation. It is defined in control volume as [20]

$$\dot{s}_{gen} = \frac{1}{m} \int \left(\frac{\mu\varphi}{T} + \frac{\rho\varepsilon}{T} + \frac{\lambda \left(\nabla T\right)^2}{T^2} \right) \mathrm{d}V \ , \tag{15}$$

where m is the fluid mass in the control volume, $\mu\varphi$ is the normal viscous dissipation term, ε is the turbulence dissipation rate, V is the volume. Results of specific entropy generation rate depending on the type of heat exchanger and flow rate are presented in Tab. 9. Local minimum, at the flow rate of 200 l/h can be noticed for both cases. Moreover, increasing flow rate reveals bigger irreversibility in A type, flat geometry.

The volumetric vorticity, defined in [20], was also taken into account to identify, which geometry caused stronger flow structure modification. As it can be noticed from Tab. 9, the geometry of A type caused more visible modification of the flow.

5 Summary

Presented work considers flow and thermal phenomena occurring in the system consisting of one single-phase minijet as well as minijets array, and surfaces (flat and concave) heated with constant heat flux. Numerical analyses, based on the mass, momentum and energy conservation laws, were

Table 9: Production of entropy and volumetric vorticity values.

Volumetric flow rate, l/h	Corresponding mean Re in the orifice	Rate of specific entropy generation, W/(kg K)		Vorticity, 1/s	
		Type A	Type B	Type A	Type B
100	1115	2.77	2.78	7.54E-4	6.70E-4
200	2260	2.05	2.06	1.57E-3	1.34E-3
300	3430	2.35	2.30	2.42E-3	2.02E-3
400	4600	3.58	3.51	3.31E-3	2.74E-3

conducted. Shape of impinged surface was treated as the main factor of comparison. RANS-based models were used – having some drawbacks in overall accuracy, however sufficient to determine for example relations between particular geometric, thermal and hydraulic parameters. Obtained results can be a starting point for further, e.g., LES-based, analyses.

When comparing results of single-phase individual minijets and their arrays, it can be noticed, that different phenomena occurred, impacting the results. In Fig. 7 it was shown, that average values of thermal parameters were the same for both impinged heat exchanger surfaces, however such effect was not present when examining one minijet. Effect of crossflow might be a possible reason. Analyses of singular jets led to conclusion, that due to different geometry it was impossible to reach the values of stagnation Nusselt number equal to that for flat surface.

Presented research involved just small part of heat exchanger – limited to presented minijets array. It was necessary to control computation time and generated mesh elements. In global approach, however, advantages of using cylindrical shape (with hot fluid pipe inside and cold fluid pipe outside) are well known. Even though the local Nusselt number values or temperature distribution did not determine, which geometry is better, comparison of specific entropy generation rate and vorticity revealed important differences. It can be assumed, that with the increasing length of computational volume and increasing number of jets, the heat exchanger of A type (flat case) will be characterized by much higher irreversibilities and generation of turbulence, which may influence the heat transfer processes. However it is under the consideration and the results would be presented soon.

The results also demonstrated the necessity of further investigation in the field of universal correlations describing Nusselt number in such systems. In the case of analyzed geometries more parameters, than presented in equations from Tab. 4, should be taken into account to obtain appropriate correlations.

Acknowledgements The present work was supported by the Polish Ministry of Science (Grant AGH No. 15.11.210.390) and by PLGrid Infrastructure.

Received 15 December 2017

References

[1] Landelle A., Tauveron N., Haberschill P., Revellin R., Colasson S.: *Organic Rankine cycle design and performance comparison based on experimental database.* Appl. Energ. **204**(2017), 1172–1187.

[2] Wajs J., Mikielewicz D., Bajor M., Kneba Z.: *Experimental investigation of domestic micro-CHP based on the gas boiler fitted with ORC module.* Arch. Thermodyn. **37**(2016), 3, 79–93.

[3] Wajs J., Mikielewicz D., Fornalik-Wajs E.: *Cylindrical jet heat exchanger dedicated to heat recovery, especially from low temperature waste sources.* Patent PL224494, 2013 (in Polish).

[4] Wajs J., Mikielewicz D., Fornalik-Wajs E., Bajor M.: *Recuperator with microjet technology as a proposal for heat recovery from low-temperature sources.* Arch. Thermodyn. **36**(2015), 4, 48–63.

[5] Wajs J., Mikielewicz D., Fornalik-Wajs E., Bajor M.: *High performance tubular heat exchanger with minijet heat transfer enhancement.* Heat Transfer Eng. doi: 10.1080/01457632.2018.1442369

[6] Tong A.Y.: *A numerical study on the hydrodynamics and heat transfer of a circular liquid jet impinging onto a surface.* Numer. Heat Tr. A-Appl. **44**(2003), 1, 1–19.

[7] Berberović E., Šikalo Š.: *Computational modelling and simulation of nonisothermal free-surface flow of a liquid jet impinging on a heated surface.* Procedia Engineering **100**(2015), 115-124.

[8] Stevens J., Webb B.W.: *Measurements of the free surface flow structure under an impinging, free liquid jet.* J. Heat Trans-T. ASME **114**(1992), 1, 79–84.

[9] Liu X., Lienhard J.H., Lombara J.S.: *Convective heat transfer by impingement of circular liquid jets.* J. Heat Trans-T. ASME **113**(1991), 571–582.

[10] Zuckerman N., Lior N.: *Jet impingement heat transfer: physics, correlations, and numerical modeling.* Adv. Heat Transfer **39**(2006), 565–631.

[11] Choo K., Friedrich B.K., Glaspell A.W., Schilling K.A.: *The influence of orifice-to-plate spacing on heat transfer and fluid flow of submerged jet impingement.* Int. J. Heat Mass Tran. **97**(2016), 66–69.

[12] Yasaswy N.S., Saroj S., Hindasageri V., Prabhu S.V.: *Local heat transfer distribution of an impinging air jet through a crossflow.* Int. J. Therm. Sci. **79**(2014), 250–259.

[13] Lee J., Ren Z., Ligrani P., Fox M.D., Moon H.-K.: *Crossflows from jet array impingement cooling: Hole spacing, target plate distance, Reynolds number effects.* Int. J. Therm. Sci. **88**(2015), 7–18.

[14] Draksler M., Končar B., Cizelj L., Ničeno B.:*Large Eddy Simulation of multiple impinging jets in hexagonal configuration – Flow dynamics and heat transfer characteristics.* Int. J. Heat Mass Tran. **109**(2017), 16–27.

[15] ANSYS, Inc.: *ANSYS FLUENT Theory Guide, Release 14.5.* Canonsburg 2012.

[16] Brdlik P.M., Savin V.K.: *Heat transfer between an axisymmetric jet and a plate normal to the flow.* J. Eng. Phys. **8**(1965), 2, 91–98.

[17] Womac D.J., Ramadhyani S., Incropera F.P.: *Correlating equations for impingement cooling of small heat sources with single circular liquid jets.* J. Heat Trans-T. ASME **115**(1993), 1, 106–115.

[18] Robinson A.J., Schnitzler E.: *An experimental investigation of free and submerged miniature liquid jet array impingement heat transfer.* Exp. Therm. Fluid Sci. **32**(2007), 1, 1–13.

[19] Fabbri M., Dhir V.K.: *Optimized heat transfer for high power electronic cooling using arrays of microjets.* J. Heat Trans-T. ASME **127**(2005), 7, 760–769.

[20] Bejan A.: *Entropy minimization: the new thermodynamics of finite-size devices and finite-time processes.* J. Appl. Phys. **79**(1996), 3, 1191–1218.